JACS
JOURNAL OF THE AMERICAN CHEMICAL SOCIETY

Communication

pubs.acs.org/JACS

Detailed Structure of the $H_2PO_4^-$–Guanosine Diphosphate Intermediate in Ras-GAP Decoded from FTIR Experiments by Biomolecular Simulations

Fei Xia,[†,‡] Till Rudack,[#,‡] Qiang Cui,[⊥] Carsten Kötting,[#] and Klaus Gerwert*[,†,#]

[†]Chinese Academy of Sciences–Max Planck Partner Institute and Key Laboratory for Computational Biology, Shanghai Institutes for Biological Sciences, 320 Yue Yang Road, Shanghai, 200031, China

[#]Department of Biophysics, Ruhr University Bochum, ND 04 North, 44780 Bochum, Germany

[⊥]Department of Chemistry and Theoretical Chemistry Institute, University of Wisconsin, 1101 University Avenue, Madison, Wisconsin 53706, United States

Supporting Information

ABSTRACT: Essential biochemical processes such as signal transduction, energy conversion, or substrate conversion depend on transient ligand binding. Thus, identifying the detailed structure and transient positioning of small ligands, and their stabilization by the surrounding protein, is of great importance. In this study, by decoding information from Fourier transform infrared (FTIR) spectra with biomolecular simulation methods, we identify the precise position and hydrogen network of a small compound, the guanosine diphosphate (GDP)–$H_2PO_4^-$ intermediate, in the surrounding protein–protein complex of Ras and its GTPase-activating protein, a central molecular switch in cellular signal transduction. We validate the simulated structure by comparing the calculated fingerprint vibrational modes of $H_2PO_4^-$ with those obtained from FTIR experiments. The new structural information, below the resolution of X-ray structural analysis, gives detailed insight into the catalytic mechanism.

Regulation of many cellular processes by guanosine triphosphate (GTP) hydrolysis is crucial in living cells, and its interference causes several diseases.[1] GTP hydrolysis is catalyzed by enzymes like the small GTPase Ras p21, which switches from the active to the inactive conformation and terminates signal transduction by hydrolytically cleaving the substrate, GTP, to guanosine diphosphate (GDP) and inorganic phosphate (P_i).[2,3] To control cell growth, ~10^{10}-fold acceleration of GTP hydrolysis (50 ms vs 200 d in water) is accomplished via complex formation with Ras and a GTPase-activating protein (GAP).[2,4] Malfunctions associated with constitutively active Ras can cause tumors.[5,6] Therefore, mechanisms of GTP hydrolysis and its catalysis by Ras have been intensively studied using various theoretical[4,7−14] and experimental[15−22] approaches in recent decades.

Fourier transform infrared (FTIR) spectroscopy is very sensitive to structural details that are beyond the resolution of X-ray crystallography, which is necessary to understand catalysis.[4] There are two available X-ray structures of GDP·P_i bound to a small GTPase without the corresponding GAP: one bound to Rab11aQ70L (PDB ID: 1OIX)[23] and one to Di-Ras2 (PDB ID: 2ERX).[24] It is unclear whether these static structures are real intermediates along the reaction pathway or artificially formed under the crystallization conditions. Recently, FTIR studies discovered the existence of a stable GDP·$H_2PO_4^-$ intermediate bound to Ras·GAP.[22] However, the structural information has to be decoded from the specific vibrational modes of substrates in proteins. Recent studies have shown that small but decisive changes in structure and charge distribution can be detected by the combination of biomolecular simulations and FTIR spectroscopy.[4,25] These studies focused on substrate changes in the educt and product states in different environments. Here, by combining FTIR and biomolecular simulations, we identify a transient state during the reaction pathway of a small compound, thereby closing an important gap in the GTP hydrolysis reaction pathway: the structure of GDP·$H_2PO_4^-$ within the Ras·GAP complex, the central intermediate during GTP hydrolysis. The rate-limiting step in this reaction is the release of inorganic phosphate into the bulk. Theoretical studies of GTP hydrolysis consider this structure the product and not an intermediate. By monitoring time-resolved IR absorbance changes, we can follow the hydrolysis of GTP to GDP in Ras on the millisecond time scale.[26] The variations of specific vibrational bands with time indicate the cleavage of the γ-phosphate and the formation of chemical bonds.[22] FTIR investigations can therefore reveal reaction mechanisms and allow us to derive the reaction rate constants of GTP hydrolysis.[27]

Many theoretical studies have investigated the reaction pathway of GTP hydrolysis in Ras·GAP, but there are only a few[8,11−13] with reasonable activation barriers in agreement with the experimental results. These theoretical studies consider only bond breakage, and therefore the product state of the simulations is the intermediate state GDP·$H_2PO_4^-$. Regarding biological function, the complete reaction pathway has to be considered because Ras is still in the signal-transducing "on" state within the intermediate,[28] but not in the "off" state, which inhibits signal transduction. In principle, structural information about the intermediate could be obtained from these studies,

Received: October 24, 2012
Published: November 26, 2012

dx.doi.org/10.1021/ja310496e | J. Am. Chem. Soc. 2012, 134, 20041−20044

but they all focus on the transition state and the activation barrier, because this is the only reliable observable for the whole reaction pathway that can be compared to experimental results. However, precise validation of the educt and product structures is important; agreement of the activation barriers is not sufficient proof of the intermediate structure. By calculating vibrational modes and comparing to measured values, we are able to explicitly validate the intermediate structure, which has not yet been observed by X-ray experiments for wild-type Ras or Ras-like proteins in complex with GAP.

Detailed knowledge of the intermediate structure is crucial to understand the subsequent steps of hydrolysis. We need structural clarification of why the intermediate is in the "on" state[28] and why the rate-limiting step for hydrolysis is $H_2PO_4^-$ release.[22] Here, we describe the intermediate structure obtained by self-consistent charge−density functional tight-binding (SCC-DFTB)[29] optimized for phosphate hydrolysis reactions[30] with umbrella sampling[31] and further refinement by molecular mechanics (MM) and quantum mechanics/molecular mechanics (QM/MM) simulations. The calculated spectroscopic features of $H_2PO_4^-$ fit the spectroscopic results and validate this intermediate structure.

As a starting structure, we used the X-ray structure of Ras·GAP·GDP·AlF_3 (PDB ID: 1WQ1).[16] GDP·AlF_3 is an analogue for the transition state of GTP hydrolysis and therefore the most reasonable accessible starting structure. We replaced GDP·AlF_3 by GTP and amended the X-ray structure in a manner similar to that reported by Rudack et al.[25] We used the MM-equilibrated reactant conformation of Ras·GAP·GTP and allowed GTP hydrolysis to proceed toward the intermediate state by umbrella sampling.[31] The reaction pathway is analogous to that of ATP hydrolysis in myosin.[32] First, the nucleophilic attacking water transfers one hydrogen atom to the oxygen atom of the γ-phosphate and then attacks the phosphorus atoms of the γ-phosphate to form the inorganic molecule $H_2PO_4^-$ (Figure S1). This protonation state was already revealed clearly by FTIR experiments.[22] With the GDP·$H_2PO_4^-$ intermediate bound to Ras·GAP, we performed a 50 ns MM simulation using the CHARMM force fields and the GROMACS 4.0.7 program suite.[33,34] The system reached equilibrium in 10 ns. To further refine the intermediate structure, this snapshot at 10 ns was taken as the starting structure for another 50 ps QM/MM simulation. We calculated normal modes for each picosecond of the first 10 ps of the QM/MM trajectory. The deviation for each vibrational mode among the 10 snapshots is within the spectral bandwidth area (Table S1). Therefore, the QM/MM trajectory reveals a stable conformation. For normal-mode analysis, we used the same approach as in previous studies.[35] A detailed description of the simulation setup and parameters, including the program suites used, is in the Supporting Information.

Two of the specific P−O stretching modes of $H_2PO_4^-$ have been experimentally resolved (Figure 1). All other vibrational modes of $H_2PO_4^-$ have lower absorption coefficients and are in a region with poor signal-to-noise ratio. The calculated antisymmetric vibrational mode $\nu_a(PO_2)$ (1202 cm^{-1}) fits the experimentally assigned frequency of 1186 cm^{-1} within the error of the method (~2% ≙ 25 cm^{-1}). The calculated symmetric vibrational mode $\nu_s(PO_2)$ (1093 cm^{-1}) fits the experimental value of 1113 cm^{-1}. Further, we calculated the influence of γ-$^{18}O_4$, β-$^{18}O_4$, and β-$^{18}O_1$ isotopic labeling (Figure S2) on the vibrational modes of $H_2PO_4^-$ and compared them to the experiment. These relative shifts, which reflect the

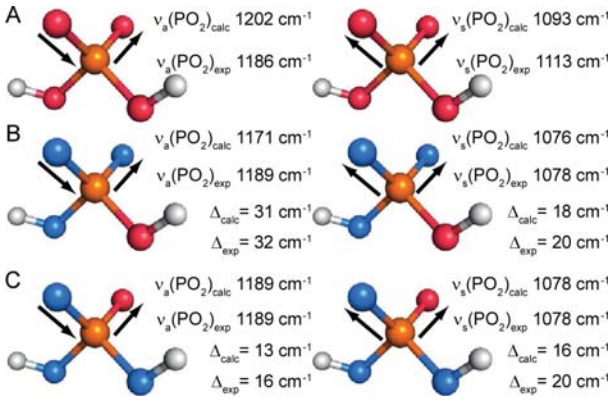

Figure 1. Comparison of the calculated and experimental specific P−O stretching modes of $H_2PO_4^-$ without (A) and with (B,C) γ-$^{18}O_4$ labeling. The red atoms are ^{16}O and the blue ones ^{18}O. The calculated values are averaged over 10 snapshots (Table S1).

character of the normal-mode vibration, can be calculated with greater accuracy than the absolute frequencies. In isotopic labeling experiments of γ-$^{18}O_4$ and β-$^{18}O_1$, one of the three nonbridging oxygen atoms of the β-phosphate is labeled. Since the barrier for β-phosphate group rotation is low, the label is distributed among all three positions. In our calculations we tested all possibilities and found no significant differences for each of the nonbridging oxygen atoms of the β-phosphate. If one hydroxyl oxygen atom and two single oxygen atoms of $H_2PO_4^-$ are labeled (Figure 1B), $\nu_a(PO_2)$ shifts 31 cm^{-1} and $\nu_s(PO_2)$ 18 cm^{-1}, in accordance with the experimental values of 32 and 20 cm^{-1}, respectively.[22] If one oxygen atom and two hydroxyl oxygen atoms are labeled (Figure 1C), $\nu_a(PO_2)$ shifts 13 cm^{-1} and $\nu_s(PO_2)$ 16 cm^{-1}, in accordance with the experimental values of 16 and 20 cm^{-1}, respectively.[22] Calculated band shifts for $\nu_s(PO_2)$ with β-$^{18}O_1$ and β-$^{18}O_4$ isotope labeling are 7 and 17 cm^{-1}, in good agreement with the experimental values of 5 and 12 cm^{-1}, respectively.[22] This shift in vibrations of cleaved $H_2PO_4^-$ upon GDP labeling is due to coupling of vibrational modes and indicates that $H_2PO_4^-$ is still in close proximity to GDP. In the calculated vibrational modes, a clear through-space coupling between $\nu_s(PO_2)$ of $H_2PO_4^-$ and $\nu_a(PO_3)_\beta$ of GDP can be observed. Therefore, IR spectroscopy can be used for distance estimations, similar to nuclear magnetic resonance spectroscopy. Furthermore, the differences between the vibrational modes for $H_2PO_4^-$ in water (calculated,[36] $\nu_a(PO_2)$ = 1153 cm^{-1}, $\nu_s(PO_2)$ = 1068 cm^{-1}; measured,[37] $\nu_a(PO_2)$ = 1156 cm^{-1}, $\nu_s(PO_2)$ = 1077 cm^{-1}) and bound to Ras·GAP reveal that the spectra are sensitive to the particular hydrogen bond network. Besides the $H_2PO_4^-$ vibrational modes, we identified an antisymmetric and a symmetric vibrational mode for the α- and β-phosphate, denoted as $\nu_{a/s}(PO_2)_\alpha$ and $\nu_{a/s}(PO_3)_\beta$ (Table S1).

In summary, we show that the fingerprint vibrational modes and isotopic shifts of $H_2PO_4^-$ fit the experimental results well within the error of the method. The strong coupling between $H_2PO_4^-$ and GDP underlines the accordance between calculated and experimental spectral features. Therefore, a detailed analysis of our intermediate structure gained by biomolecular simulations is justified.

The upper limit for the distance between the $H_2PO_4^-$ phosphorus and that of the β-phosphate was proposed as 5.0 Å.[22] Our 50 ns MM simulation reveals an equilibrium

dx.doi.org/10.1021/ja310496e | J. Am. Chem. Soc. 2012, 134, 20041−20044

distance d (Figure 2) of 4.0 ± 0.1 Å (Figure S3). This is confirmed by the distance of 4.1 ± 0.1 Å during the 50 ps QM/MM simulation run. A similar distance was found in the X-ray structure of the GDP·P_i intermediate in Rab11aQ70L (4.0 Å)[23] and Di-Ras2 (4.2 Å). Computational studies report a distance of 4.1 Å.[13] This distance is stabilized by contacts between all three nonbridging oxygen atoms of the β-phosphate with $H_2PO_4^-$ (Figure 2). One of the two hydrogen atoms of $H_2PO_4^-$ forms a hydrogen bond with the β-phosphate. Further, an oxygen atom of $H_2PO_4^-$ and one of the β-phosphate coordinate the Mg^{2+}. The last nonbridging oxygen atom of the β-phosphate is connected to $H_2PO_4^-$ via Lys16. Interactions with Lys16 and Mg^{2+} are present in both X-ray structures. Due to the strong connection between $H_2PO_4^-$ and the β-phosphate, the oxygen atoms remain in an almost eclipsed position, which is a prerequisite for the experimentally and computationally observed coupling of the $H_2PO_4^-$ and GDP vibrations.[22] The β- and α-phosphate oxygen atoms are staggered because Arg789 only binds the α-phosphate and does not stabilize an eclipsed conformation by the connecting γ- and α-phosphates, as observed in the educt state.[4]

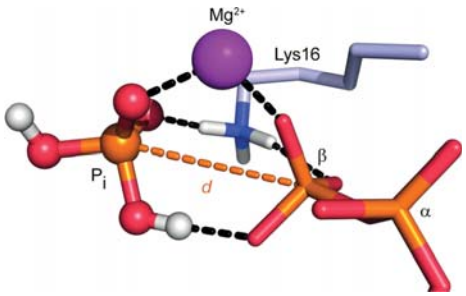

Figure 2. Interactions between the $H_2PO_4^-$ and GDP in the intermediate state in Ras·GAP. The $H_2PO_4^-$ still has strong interactions with the β-phosphate of the GDP.

$H_2PO_4^-$ is not only strongly bound to the β-phosphate but also embedded in the Ras active site by a strong hydrogen bond network (Figure 3A). Thr35, a marker for the conformational change from active to inactive Ras,[38] still coordinates the Mg^{2+}, in contrast to the product state. Furthermore, the backbone oxygen and nitrogen atoms of Thr35 each form a hydrogen bond with $H_2PO_4^-$, as also in the educt state for the γ-phosphate. This Thr35 binding motif is also observed by reaction pathway studies.[11] Gly60 directly and Gln61 via a water molecule complete the strong hydrogen bond network of $H_2PO_4^-$. The connection of Gln61 via a water molecule to $H_2PO_4^-$ can also be seen in the structure reported by Grigorenko et al.,[13] resulting from reaction pathway calculations. In the educt, the same interactions are also formed between Gly60, Gln61, and the γ-phosphate. The hydrogen bonds of the conserved amino acids Thr35 and Gly60 are also found in the X-ray structures of the intermediate in Rab11aQ70L (Thr43, Gly69) and Di-Ras2 (Thr39, Gly 64). In both, Gln61 is not present at the equivalent position, and no interaction of the corresponding amino acid (Leu70, Ser65) with $H_2PO_4^-$ is seen. Overall, the hydrogen network of the intermediate state is very close to that of the educt state. This fits the experimental observation that the intermediate is an "on" state.[28]

The intermediate separates the first reaction step of bond cleavage and the second one of charge segregation of $H_2PO_4^-$ from the Lys16 and Mg^{2+}, lowering the activation barrier for hydrolysis and facilitating significant back reaction from the intermediate toward GTP. Interestingly, an intermediate state could not be observed in every GTPase. However, we assume that such an intermediate exists in all reaction pathways but is resolved only when product formation is faster than its decay. Even if there is an intermediate, the spectral features deviate, indicating different positioning of $H_2PO_4^-$ among different GTPases, which might effect different hydrolysis rates. Furthermore, the existence of such a strong hydrogen bond network in the intermediate state is another indication that $H_2PO_4^-$ release is the rate-limiting step in hydrolysis.

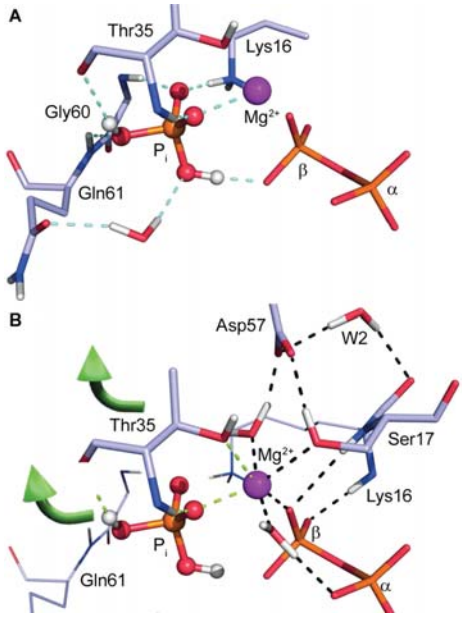

Figure 3. Detailed structure of the active center of Ras·GAP in the GDP·$H_2PO_4^-$ intermediate state, obtained from biomolecular simulations. (A) The hydrogen-bonding network of $H_2PO_4^-$, which is strongly embedded, similar to the educt state. This explains why the intermediate state is an "on" state and why $H_2PO_4^-$ release is the rate-limiting step in GTP hydrolysis. (B) Extended view of the same state showing the Mg^{2+} being bound to GDP via a strong hydrogen bond network (black dashed lines), whereas Thr35 and $H_2PO_4^-$ are only loosely bound to Mg^{2+} (green dashed lines). This explains why Thr35 is no longer bound to Mg^{2+} after $H_2PO_4^-$ release.

The interaction network of Mg^{2+} (Figure 3B) sheds further light on Thr35 movement and $H_2PO_4^-$ release. Thr35 has only one interaction with Mg^{2+} (Figure 3B, green dashed line), but it has two hydrogen bonds to $H_2PO_4^-$. GDP and $H_2PO_4^-$ both coordinate the Mg^{2+} by one oxygen atom, but the remaining three coordination partners (two waters and Ser17) develop a strong hydrogen bond network with GDP (Figure 3B, black dashed lines). One coordinating water is hydrogen-bonded to the α-phosphate; the other participates in the hydrogen bond network between Asp57, Ser17, and Lys16 by forming a hydrogen bond with the carboxyl group of Asp57. The other carboxyl oxygen of Asp57 forms a hydrogen bond with the hydroxyl group of Ser17. This guarantees maximal electrostatic interaction of Ser17 and the water molecule with the Mg^{2+} and prevents the possible mismatching of hydrogen bonding with other residues. Furthermore, Asp57 and Lys16 are connected via a water molecule. The stabilizing role of this water has been emphasized by recent studies[39] as well. The backbone nitrogen

dx.doi.org/10.1021/ja310496e | J. Am. Chem. Soc. 2012, 134, 20041−20044

atoms of Lys16 and Ser17 form hydrogen bonds with the β-phosphate. This interaction network provides a very strong connection between Mg^{2+} and GDP. The importance of this network in the educt state has already been shown using mutagenesis. The S17A and D57A mutations achieve a 30- and 16-fold decrease in Mg^{2+} binding affinity, respectively.[40] The interaction of Thr35 with Mg^{2+} is not as strong as that of Ser17. The T35A mutation does not significantly affect Mg^{2+} binding affinity.[40] In accordance with the experiments, the distance averaged over the 50 ps QM/MM trajectory between the hydroxyl oxygen atom of Thr35 and the Mg^{2+} is larger with a higher fluctuation (2.46 ± 0.36 Å) compared to the distance between the hydroxyl oxygen atom of Ser17 and Mg^{2+} (2.16 ± 0.17 Å). Compared to the educt state (2.17 ± 0.02 Å),[25] the interaction of Thr35 with Mg^{2+} is weakened. This phenomenon is observed for ATP hydrolysis in myosin,[41] as well. All in all, this explains the outward movement of Thr35 with $H_2PO_4^-$ release, whereas the Mg^{2+} remains stably coordinated at the GDP.

In conclusion, we identified the structural details of the GDP·$H_2PO_4^-$ intermediate state in GTP hydrolysis in Ras·GAP. Knowledge of the hydrogen-bonding network of the active site helps to explain why the intermediate state is an "on" state and why $H_2PO_4^-$ release is the rate-limiting step. In addition, we understand why Thr35 moves outward with $H_2PO_4^-$. Furthermore, the intermediate structure underlines the crucial catalytic concept of separation of bond cleavage and charge segregation. We demonstrated our ability to decode transient positioning and the detailed hydrogen-bonding network of a small compound in a protein environment from FTIR spectra by biomolecular simulations. Identifying the positioning of small compounds is crucial for targeted drug design.

■ ASSOCIATED CONTENT

Supporting Information

Setup of simulation systems, parameters, software, and procedure. This material is available free of charge via the Internet at http://pubs.acs.org.

■ AUTHOR INFORMATION

Corresponding Author

gerwert@bph.rub.de

Author Contributions

‡X.F. and T.R. contributed equally to this work.

Notes

The authors declare no competing financial interest.

■ ACKNOWLEDGMENTS

We thank the Fund for Young Talents Frontier Project (2011KIP310), Shanghai Institutes for Biological Sciences, and the Deutsche Forschungsgemeinschaft for financial support (SFB642). We thank Jürgen Schlitter for fruitful discussions and Guanhua Hou for providing the phosphate parameters for the CHARMM force field.

■ REFERENCES

(1) Maegley, K. A.; Admiraal, S. J.; Herschlag, D. *Proc. Natl. Acad. Sci. U.S.A.* **1996**, *93*, 8160.
(2) Vetter, I. R.; Wittinghofer, A. *Science* **2001**, *294*, 1299.
(3) Wittinghofer, A.; Vetter, I. R. *Annu. Rev. Biochem.* **2011**, *80*, 943.
(4) Rudack, T.; Xia, F.; Schlitter, J.; Kötting, C.; Gerwert, K. *Proc. Natl. Acad. Sci. U.S.A.* **2012**, *109*, 15295.
(5) Cox, A. D.; Der, C. J. *Small GTPases* **2010**, *1*, 2.
(6) Wittinghofer, A.; Waldmann, H. *Angew. Chem., Int. Ed.* **2000**, *39*, 4192.
(7) Futatsugi, N.; Hata, M.; Hoshino, T.; Tsuda, M. *Biophys. J.* **1999**, *77*, 3287.
(8) Glennon, T. M.; Villa, J.; Warshel, A. *Biochemistry* **2000**, *39*, 9641.
(9) Kosztin, I.; Bruinsma, R.; O'Lague, P.; Schulten, K. *Proc. Natl. Acad. Sci. U.S.A.* **2002**, *99*, 3575.
(10) Cavalli, A.; Carloni, P. *J. Am. Chem. Soc.* **2002**, *124*, 3763.
(11) Grigorenko, B. L.; Nemukhin, A. V.; Topol, I. A.; Cachau, R. E.; Burt, S. K. *Proteins* **2005**, *60*, 495.
(12) Klähn, M.; Rosta, E.; Warshel, A. *J. Am. Chem. Soc.* **2006**, *128*, 15310.
(13) Grigorenko, B. L.; Nemukhin, A. V.; Shadrina, M. S.; Topol, I. A.; Burt, S. K. *Proteins* **2007**, *66*, 456.
(14) Grant, B. J.; Gorfe, A. A.; McCammon, J. A. *Plos Comput. Biol.* **2009**, *5*, e100325.
(15) Pai, E. F.; Krengel, U.; Petsko, G. A.; Goody, R. S.; Kabsch, W.; Wittinghofer, A. *EMBO J.* **1990**, *9*, 2351.
(16) Scheffzek, K.; Ahmadian, M. R.; Kabsch, W.; Wiesmuller, L.; Lautwein, A.; Schmitz, F.; Wittinghofer, A. *Science* **1997**, *277*, 333.
(17) Scheidig, A. J.; Burmester, C.; Goody, R. S. *Struct. Fold. Des.* **1999**, *7*, 1311.
(18) Schweins, T.; Geyer, M.; Scheffzek, K.; Warshel, A.; Kalbitzer, H. R.; Wittinghofer, A. *Nat. Struct. Biol.* **1995**, *2*, 36.
(19) Spoerner, M.; Hozsa, C.; Poetzl, J. A.; Reiss, K.; Ganser, P.; Geyer, M.; Kalbitzer, H. R. *J. Biol. Chem.* **2010**, *285*, 39768.
(20) Wang, J. H.; Xiao, D. G.; Deng, H.; Callender, R.; Webb, M. R. *Biospectroscopy* **1998**, *4*, 219.
(21) Allin, C.; Gerwert, K. *Biochemistry* **2001**, *40*, 3037.
(22) Kötting, C.; Blessenohl, M.; Suveyzdis, Y.; Goody, R.; Wittinghofer, A.; Gerwert, K. *Proc. Natl. Acad. Sci. U.S.A.* **2006**, *103*, 13911.
(23) Pasqualato, S.; Cherfils, J. *Structure* **2005**, *13*, 533.
(24) Papagrigoriou, E.; Yang, X.; Elkins, J.; Niesen, F. E.; Burgess, N.; Salah, E.; Fedorov, O.; Ball, L. J.; von Delft, F.; Sundstrom, M.; Edwards, A.; Arrowsmith, C.; Weigelt, J.; Doyle, D. *RCSB PDB* **2005**, DOI: 10.2210/pdb2erx/pdb.
(25) Rudack, T.; Xia, F.; Schlitter, J.; Kötting, C.; Gerwert, K. *Biophys. J.* **2012**, *103*, 293.
(26) Cepus, V.; Scheidig, A. J.; Goody, R. S.; Gerwert, K. *Biochemistry* **1998**, *37*, 10263.
(27) Kötting, C.; Gerwert, K. *Chem. Phys.* **2004**, *307*, 227.
(28) Kötting, C.; Kallenbach, A.; Suveyzdis, Y.; Wittinghofer, A.; Gerwert, K. *Proc. Natl. Acad. Sci. U.S.A.* **2008**, *105*, 6260.
(29) Elstner, M.; Porezag, D.; Jungnickel, G.; Elsner, J.; Haugk, M.; Frauenheim, T.; Suhai, S.; Seifert, G. *Phys. Rev. B* **1998**, *58*, 7260.
(30) Yang, Y.; Yu, H. B.; York, D.; Elstner, M.; Cui, Q. *J. Chem. Theory Comput.* **2008**, *4*, 2067.
(31) Torrie, G. M.; Valleau, J. P. *J. Comput. Phys.* **1977**, *23*, 187.
(32) Yang, Y.; Yu, H. B.; Cui, Q. *J. Mol. Biol.* **2008**, *381*, 1407.
(33) Van der Spoel, D.; Lindahl, E.; Hess, B.; Groenhof, G.; Mark, A. E.; Berendsen, H. J. C. *J. Comput. Chem.* **2005**, *26*, 1701.
(34) Hess, B.; Kutzner, C.; van der Spoel, D.; Lindahl, E. *J. Chem. Theory Comput.* **2008**, *4*, 435.
(35) Xia, F.; Rudack, T.; Kötting, C.; Schlitter, J.; Gerwert, K. *Phys. Chem. Chem. Phys.* **2011**, *13*, 21451.
(36) VandeVondele, J.; Troster, P.; Tavan, P.; Mathias, G. *J. Phys. Chem. A* **2012**, *116*, 2466.
(37) Klähn, M.; Mathias, G.; Kötting, C.; Nonella, M.; Schlitter, J.; Gerwert, K.; Tavan, P. *J. Phys. Chem. A* **2004**, *108*, 6186.
(38) Kötting, C.; Kallenbach, A.; Suveyzdis, Y.; Eichholz, C.; Gerwert, K. *ChemBioChem* **2007**, *8*, 781.
(39) Prakash, P.; Sayyed-Ahmad, A.; Gorfe, A. A. *Plos Comput. Biol.* **2012**, *8*, e1002394.
(40) John, J.; Rensland, H.; Schlichting, I.; Vetter, I.; Borasio, G. D.; Goody, R. S.; Wittinghofer, A. *J. Biol. Chem.* **1993**, *268*, 923.
(41) Yu, H. B.; Ma, L.; Yang, Y.; Cui, Q. *Plos Comput. Biol.* **2007**, *3*, 199.

Supporting Information

Detailed Structure of the $H_2PO_4^-$Guanosine Diphosphate Intermediate in Ras-GAP Decoded from FTIR Experiments by Biomolecular Simulations

Fei Xia[†,‡], Till Rudack[#,‡], Qiang Cui[⊥], Carsten Kötting[#], Klaus Gerwert[†,#,*]

[†]Chinese Academy of Sciences-Max Planck Partner Institute and Key Laboratory for Computational Biology, Shanghai Institutes for Biological Sciences, 320 Yue Yang Road, Shanghai, 200031, China

[#]Department of Biophysics, Ruhr University Bochum, ND 04 North, 44780 Bochum, Germany

[⊥]Department of Chemistry and Theoretical Chemistry Institute, University of Wisconsin, 1101 University Avenue, Madison, Wisconsin 53706, USA

SCC-DFTBPR/MM simulation with umbrella sampling

We performed self-consistent-charge-density-functional-tight-binding[1] / molecular mechanics (SCC-DFTB/MM) simulation with umbrella sampling[2] with the CHARMM program suit.[3] We used the SCC-DFTB method with optimized parameters for hydrolysis reactions involving phosphorus atoms (SCC-DFTBPR).[4] As a starting structure, we used the X-ray structure of Ras·GAP·GDP·AlF_3 (PDB ID: 1WQ1[5]). GDP·AlF_3 is an analog for the transition state of GTP hydrolysis and therefore the most reasonable accessible starting structure. We replaced GDP·AlF_3 by GTP and amended the X-ray structure in a manner similar to that of Rudack *et al.*[6]. The simulation system was set up by solvating the active center of the Ras·GAP system with a water sphere with a radius of 25 Å. The electrostatic interaction of the whole system was treated with the Generalized Solvent boundary potential method.[7,8] The boundary between the quantum mechanic (QM) and molecular mechanic (MM) part is achieved by cutting the bond between the carbon atoms C5' and C4' of GTP by the link atom method.[9] The QM region compromises the triphosphate group of GTP, the Mg^{2+}, two waters coordinating Mg^{2+} and the nucleophilic attacking water being necessary for hydrolysis. In total 28 atoms were described by the SCC-DFTBPR. This method was developed especially for systems containing phosphorous atoms.[10,11] The MM part was described with the CHARMM force field.[12] The system for the substate GTP in the Ras·GAP was firstly pre-equilibrated for 500 ps with the SCC-DFTBPR/MM method. In order to reach the final hydrolysis products, we followed the similar mechanism of ATP hydrolysis in myosin[13,14] to give rise to the products GDP and $H_2PO_4^-$ with umbrella sampling technique. We defined a combined reaction coordinate (Fig. S1) with the expression Rc = R1−R2−R3 to describe the hydrolysis process, including the cleavage of P_γ-O_b bond and formation of PγOw and HwOγ bonds, as shown in Figure S1. The reaction coordinate Rc totally changes from −4.2 to −0.2 Å along the reaction pathway, which is divided into 22 overlapped windows for umbrella sampling. In each window, the SCC-DFTBPR/MM simulation was performed 100 ps by umbrella sampling with respect to the reaction coordinate Rc.

Simulation set up: MM simulations

A snapshot including the hydrolysis products GDP and $H_2PO_4^-$ was extracted from the last window of umbrella sampling. In this structure (Fig. S3), the distance between the atoms Pγ and Ob is 2.4 Å, which means a complete cleavage of the Pγ-Ob bond between γ- and β-phosphate of GTP. The Pγ-Pβ distance is 3.6 Å. The structure of this snapshot was embedded in a cubic water box with 33728 TIP3 water molecules. To mimic physiological concentration, 119 sodium cations and 103 chlorine anions were added into the water box to keep the whole system neutral. Periodic boundary conditions were applied to the cubic water box and the electronic interactions of the system were evaluated using the Fast Particle-Mesh Ewald method[15] with a grid spacing of 0.12 nm and fourth-order spline interpolation. The van der Waals interactions between atom pairs were truncated within a cutoff values of 1.0 nm. A Berendsen thermostat with a coupling constant of 0.1 ps and a Berendsen thermostat with a coupling constant of 1.0 ps were used to keep the system at a constant temperature of 300 K and 1 standard atmosphere, respectively.[16] The equilibrium simulation for the hydrolysis products of GDP

and $H_2PO_4^-$ in the Ras·GAP system was carried out using the CHARMM force field[12] in GROMACS 4.0.7[17,18]. First, the system was energy-minimized and pre-equilibrated with an integration step of 1 fs to achieve equilibrium. Finally, the equilibrated 50 ns MM trajectory was analyzed.

Simulation set up: QM/MM simulations

For QM/MM simulations and normal mode analysis we used the same approach as Fei *et al.*[19]. We used the QM/MM interface[20] for GROMACS[17,18] and Gaussian03[21] with the normal QM/MM scheme.[22] The QM atoms comprising the GDP nucleoside, the $H_2PO_4^-$ and Mg^{2+} treated at the level of B3LYP/6-311++G(d,p)[23,24] by Gaussian03[21]. The rest of the protein including the solvent is treated by MM using the CHARMM force field[12] in GROMACS[17,18].

REFERENCES

(1) Elstner, M.; Porezag, D.; Jungnickel, G.; Elsner, J.; Haugk, M.; Frauenheim, T.; Suhai, S.; Seifert, G. *Phys. Rev. B* **1998**, *58*, 7260.
(2) Torrie, G. M.; Valleau, J. P. *J. Comput. Phys.* **1977**, *23*, 187.
(3) Brooks, B. R.; Brooks, C. L.; Mackerell, A. D.; Nilsson, L.; Petrella, R. J.; Roux, B.; Won, Y.; Archontis, G.; Bartels, C.; Boresch, S.; Caflisch, A.; Caves, L.; Cui, Q.; Dinner, A. R.; Feig, M.; Fischer, S.; Gao, J.; Hodoscek, M.; Im, W.; Kuczera, K.; Lazaridis, T.; Ma, J.; Ovchinnikov, V.; Paci, E.; Pastor, R. W.; Post, C. B.; Pu, J. Z.; Schaefer, M.; Tidor, B.; Venable, R. M.; Woodcock, H. L.; Wu, X.; Yang, W.; York, D. M.; Karplus, M. *J. Comput. Chem.* **2009**, *30*, 1545.
(4) Yang, Y.; Yu, H. B.; York, D.; Elstner, M.; Cui, Q. *J. Chem. Theory Comput.* **2008**, *4*, 2067.
(5) Scheffzek, K.; Ahmadian, M. R.; Kabsch, W.; Wiesmuller, L.; Lautwein, A.; Schmitz, F.; Wittinghofer, A. *Science* **1997**, *277*, 333.
(6) Rudack, T.; Xia, F.; Schlitter, J.; Kötting, C.; Gerwert, K. *Biophys. J.* **2012**, *103*, 293.
(7) Nina, M.; Beglov, D.; Roux, B. *J. Phys. Chem. B* **1997**, *101*, 5239.
(8) Im, W.; Berneche, S.; Roux, B. *J. Chem. Phys.* **2001**, *114*, 2924.
(9) Field, M. J.; Bash, P. A.; Karplus, M. *J. Comput. Chem.* **1990**, *11*, 700.
(10) Cui, Q.; Elstner, M.; Kaxiras, E.; Frauenheim, T.; Karplus, M. *J. Phys. Chem. B* **2001**, *105*, 569.
(11) Yang, Y.; Yu, H. B.; York, D.; Cui, Q.; Elstner, M. *J. Phys. Chem. A* **2007**, *111*, 10861.
(12) MacKerell, A. D.; Bashford, D.; Bellott, M.; Dunbrack, R. L.; Evanseck, J. D.; Field, M. J.; Fischer, S.; Gao, J.; Guo, H.; Ha, S.; Joseph-McCarthy, D.; Kuchnir, L.; Kuczera, K.; Lau, F. T. K.; Mattos, C.; Michnick, S.; Ngo, T.; Nguyen, D. T.; Prodhom, B.; Reiher, W. E.; Roux, B.; Schlenkrich, M.; Smith, J. C.; Stote, R.; Straub, J.; Watanabe, M.; Wiorkiewicz-Kuczera, J.; Yin, D.; Karplus, M. *J. Phys. Chem. B* **1998**, *102*, 3586.
(13) Yang, Y.; Yu, H. B.; Cui, Q. *J. Mol. Biol.* **2008**, *381*, 1407.
(14) Li, G. H.; Cui, Q. *J. Phys. Chem. B* **2004**, *108*, 3342.
(15) Darden, T.; York, D.; Pedersen, L. *J. Chem. Phys.* **1993**, *98*, 10089.
(16) Berendsen, H. J. C.; Postma, J. P. M.; Vangunsteren, W. F.; Dinola, A.; Haak, J. R. *J. Chem. Phys.* **1984**, *81*, 3684.
(17) Hess, B.; Kutzner, C.; van der Spoel, D.; Lindahl, E. *J. Chem. Theory Comput.* **2008**, *4*, 435.
(18) Van der Spoel, D.; Lindahl, E.; Hess, B.; Groenhof, G.; Mark, A. E.; Berendsen, H. J. C. *J. Comput. Chem.* **2005**, *26*, 1701.
(19) Xia, F.; Rudack, T.; Kötting, C.; Schlitter, J.; Gerwert, K. *Phys. Chem. Chem. Phys.* **2011**, *13*, 21451.
(20) Groenhof, G.; Bouxin-Cademartory, M.; Hess, B.; De Visser, S. P.; Berendsen, H. J. C.; Olivucci, M.; Mark, A. E.; Robb, M. A. *J. Am. Chem. Soc.* **2004**, *126*, 4228.
(21) Frisch, M. J.; Trucks, G. W.; Schlegel, H. B.; Scuseria, G. E.; Robb, M. A.; Cheeseman, J. R.; J. A. Montgomery, J.; Vreven, T.; Kudin, K. N.; Burant, J. C.; Millam, J. M.; Iyengar, S. S.; Tomasi, J.; Barone, V.; Mennucci, B.; Cossi, M.; Scalmani, G.; Rega, N.; Petersson, G. A.; Nakatsuji, H.; Hada, M.; Ehara, M.; Toyota, K.; Fukuda, R.; Hasegawa, J.; Ishida, M.; Nakajima, T.; Honda, Y.; Kitao, O.; Nakai, H.; Klene, M.; Li, X.; Knox, J. E.; Hratchian, H. P.; Cross, J. B.; Adamo, C.; Jaramillo, J.; Gomperts, R.; Stratmann, R. E.; Yazyev, O.; Austin, A. J.; Cammi, R.; Pomelli, C.; Ochterski, J. W.; Ayala, P. Y.; Morokuma, K.; Voth, G. A.; Salvador, P.; Dannenberg, J. J.; Zakrzewski, V. G.; Dapprich, S.; Daniels, A. D.; Strain, M. C.; Farkas, O.; Malick, D. K.; Rabuck, A. D.; Raghavachari, K.; Foresman, J. B.; Ortiz, J. V.; Cui, Q.; Baboul, A. G.; Clifford, S.; Cioslowski, J.; Stefanov, B. B.; Liu, G.; Liashenko, A.; Piskorz, P.; Komaromi, I.; Martin, R. L.; Fox, D. J.; Keith, T.; Al-Laham, M. A.; Peng, C. Y.; Nanayakkara, A.; Challacombe, M.; Gill, P. M. W.; Johnson, B.; Chen, W.; Wong, M. W.; Gonzalez, C.; Pople, J. A.; B.04 ed.; Gaussian Inc.: Pittsburgh PA, 2003.
(22) Warshel, A.; Levitt, M. *J. Mol. Biol.* **1976**, *103*, 227.
(23) Becke, A. D. *J. Chem. Phys.* **1993**, *98*, 5648.
(24) Lee, C. T.; Yang, W. T.; Parr, R. G. *Phys. Rev. B* **1988**, *37*, 785.

Table S1 Comparison of the available experimental (column 2) and calculated (column 4-13) specific normal vibrational modes (column 1) for the diphosphate of GDP and $H_2PO_4^-$ bound to Ras·GAP for 10 snapshots. The third column gives the averaged value of all 10 snapshots. All wavenumbers are given in cm^{-1}.

Modes	Exp.	Aver.	S1	S2	S3	S4	S5	S6	S7	S8	S9	S10
$\upsilon_a(PO_2)\alpha$		1233	1231	1230	1234	1242	1240	1231	1231	1237	1229	1228
$\upsilon_a(PO_2)$	1186	1202	1199	1210	1210	1204	1198	1199	1199	1208	1195	1197
$\upsilon_a(PO_3)\beta$		1123	1121	1130	1118	1124	1114	1121	1121	1127	1122	1132
$\upsilon_s(PO_2)$	1113	1093	1090	1094	1103	1089	1108	1090	1090	1090	1088	1089
$\upsilon_s(PO_2)\alpha$		1054	1054	1053	1053	1054	1057	1054	1054	1053	1048	1059
$\upsilon_s(PO_3)\beta$		970	974	969	976	965	968	974	974	966	969	969
$\upsilon_a(PO_4)\gamma$		907	909	911	911	898	908	908	908	910	899	908
$\upsilon_s(PO_4)\gamma$		816	817	807	827	803	825	817	817	814	813	819

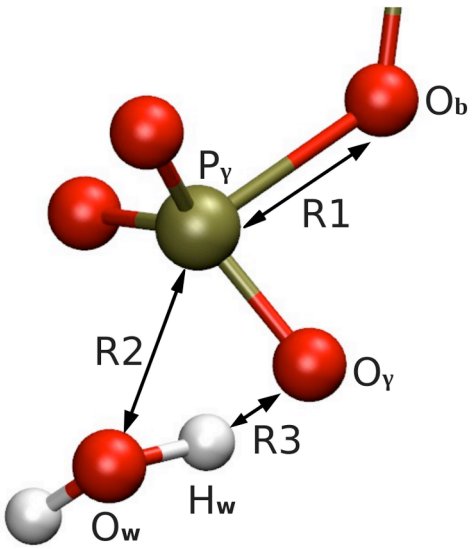

Figure S1 A combined reaction coordinate Rc=R1-R2-R3 is defined for umbrella sampling. The distances R1 is the one between the bridged oxygen atom Ob and Pγ of the γ-phosphate of GTP, R2 is the distance between the oxyen atom Ow of the nucleophillic attacking water and Pγ, and R3 the distance between the hydrogen atom Hw of the nucleophilc attaking water and the oxygen atom Oγ of the γ-phosphate.

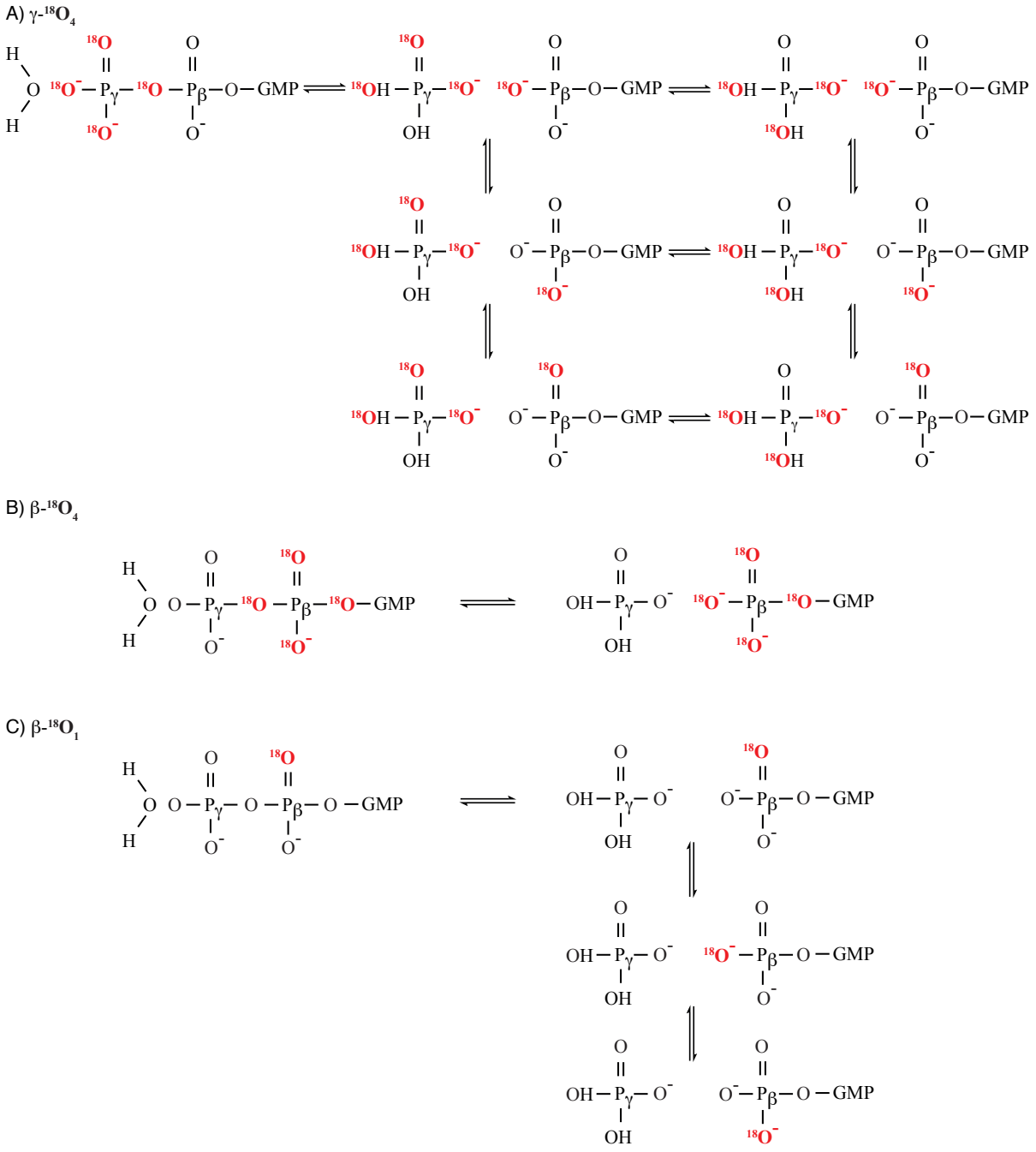

Figure S2 All possible label positions after bond cleavage using the available γ-$^{18}O_4$ (A), β-$^{18}O_4$ (B), and β-$^{18}O_1$ (C) isotopically labeled GTP, which have been measured experimentally. The vibrational modes of the isotopically labeled intermediate structures on the right side have been calculated. The isotopic shift is the difference between the average of the calculated vibrational modes of each isotopomer and the calculated vibrational mode of the non-labeled structure.

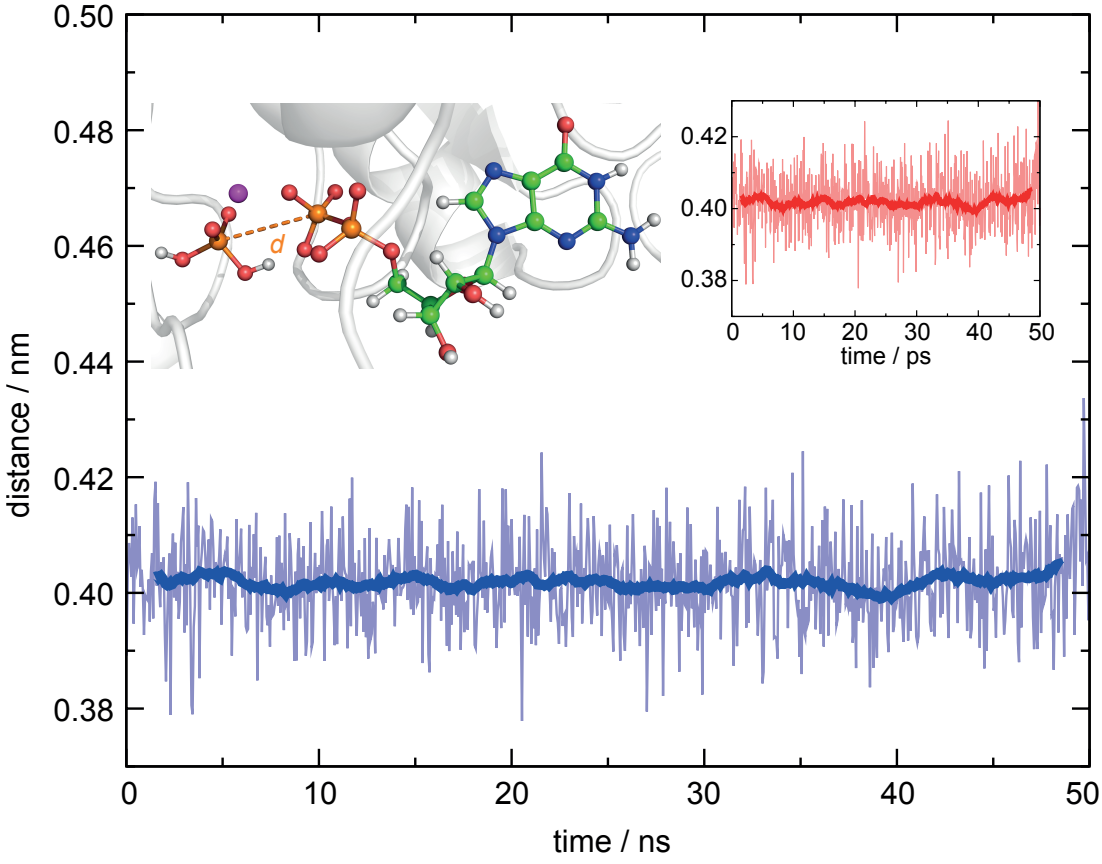

Figure S3 The distance plot of the phosphorous atom of $H_2PO_4^-$ and the phosphorous atom of the β-phosphate in Ras·GAP, extracted from the equilibrated 50 ns MM trajectory (blue graph) and the 50 ps QM/MM trajectory (red graph). The embedding shows the Mg^{2+}, $H_2PO_4^-$ and GDP molecules in Ras·GAP, with the dashed orange line denoting the plotted distance.

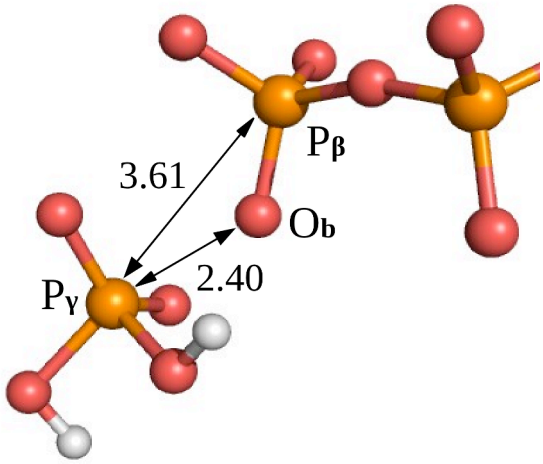

Figure S4 The structure of the hydrolysis products GDP and $H_2PO_4^-$ extracted from the last window of umbrella sampling. Shown distances are given in Ångstrom.